

Article

Impact of Multiple Module Collectors on the Cell Current Distribution within the Battery Pack

Zhihao Yu ¹, Zhezhe Sun ¹, Long Chang ^{1,2,*}, Chen Ma ^{1,2}, Changlong Li ², Hongyu Li ^{1,3}, Chunxiao Luan ¹ and Mohammad Y. M. Al-saidi ¹

¹ School of Mechanical and Electronic Engineering, Shandong University of Science and Technology, Qingdao 266590, China; zhihaoyu@sdust.edu.cn (Z.Y.); zhezhesun@sdust.edu.cn (Z.S.); machen@mail.sdu.edu.cn (C.M.); lihy@sdust.edu.cn (H.L.); skd994555@sdust.edu.cn (C.L.); skd992088@sdust.edu.cn (M.Y.M.A.-s.)

² School of Control Science and Engineering, Shandong University, Jinan 250061, China; changlongli@sdu.edu.cn

³ Key Laboratory of Marine Environmental Survey Technology and Application, Ministry of Natural Resources, Guangzhou 510000, China

* Correspondence: lchang@sdust.edu.cn

Abstract: Lithium-ion batteries are usually connected in series and parallel to form a pack for meeting the voltage and capacity requirements of energy storage systems. However, different pack configurations and battery module collector positions result in different equivalent connected resistances, leading to pack current inhomogeneity, which seriously reduces the lifetime and safety of the pack. Therefore, in order to quantitatively analyze the influence of the connected resistance on the current distribution, this study researched the initial cell current distribution of the parallel module by developing mathematical models of different configurations. Then, this study explored the influence of multiple module collector positions on the current inhomogeneity of the pack under the dynamic current condition. The results show that the inhomogeneity of cell current and discharge capacity in the pack with parallel modules connected in series can be improved by keeping each cell in a parallel module with the same distance to its module collector. Furthermore, the current homogeneity of the edge parallel modules in the pack is seriously affected by the position of the single module collector. Therefore, this study innovatively proposes the symmetrical multiple module collectors of the pack, which can greatly improve the current homogeneity of the edge parallel modules, thereby improving the lifetime and safety of the pack.

Keywords: lithium-ion battery; connected resistance; current inhomogeneity; series-parallel battery pack; pack configuration



Citation: Yu, Z.; Sun, Z.; Chang, L.; Ma, C.; Li, C.; Li, H.; Luan, C.; Al-saidi, M.Y.M. Impact of Multiple Module Collectors on the Cell Current Distribution within the Battery Pack. *Batteries* **2023**, *9*, 501. <https://doi.org/10.3390/batteries9100501>

Academic Editor: Carlos Ziebert

Received: 13 July 2023

Revised: 1 September 2023

Accepted: 20 September 2023

Published: 2 October 2023



Copyright: © 2023 by the authors. Licensee MDPI, Basel, Switzerland. This article is an open access article distributed under the terms and conditions of the Creative Commons Attribution (CC BY) license (<https://creativecommons.org/licenses/by/4.0/>).

1. Introduction

With energy utilization and environmental protection becoming the focus of world development [1,2], lithium-ion batteries are being widely used in large-scale applications [3,4] (e.g., hybrid/electric vehicles (EVs) [5] and energy storage systems (ESSs) [6]) due to their advantages in energy density, weight, volume, and service life [7]. In order to meet power and capacity requirements in these applications, hundreds of battery cells are usually connected in series and parallel to form packs [8,9]. A systematic framework for pack and application is shown in Figure 1, where pack structure includes a single cell, electrode tabs, battery frame, nickel plates, etc., and the equivalent circuit model of the pack shows the distribution of the connected resistance when scaling from battery cell to pack. However, there are multiple factors that affect the current homogeneity of the pack. These factors can be considered as differences in capacity and resistance due to the manufacturing process [10,11], the differences in module collector positions and pack configurations [12,13],

or variations in cell parameters caused by temperature, such as internal resistance, connected resistance, open-circuit voltage (OCV), etc. [14,15]. During the pack operation, the variations in the parameters affect each other to a certain extent and even amplify the inhomogeneity of the pack [16].

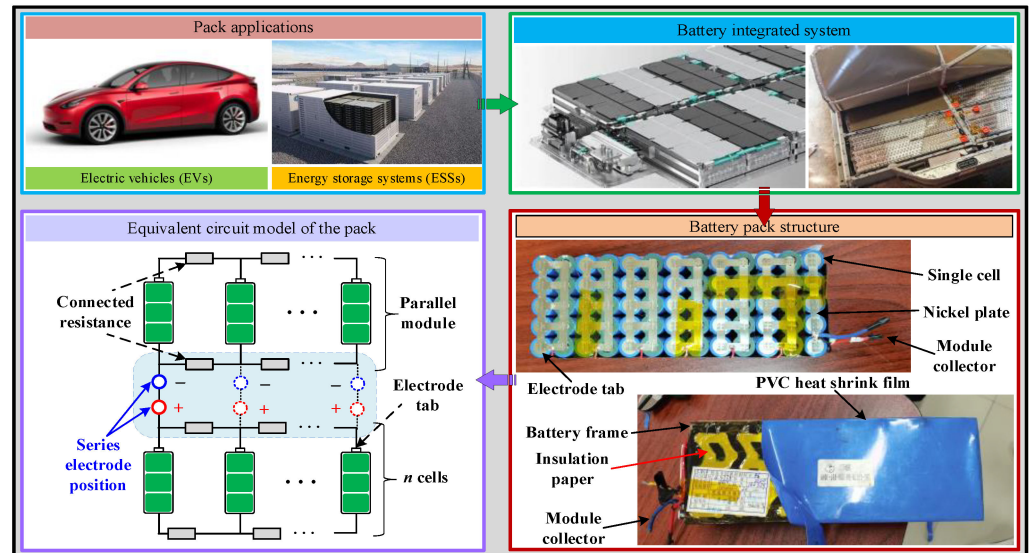


Figure 1. A systematic framework for pack and application (Including pack applications, battery integrated system, battery pack structure, and equivalent circuit model of the pack).

Focusing on connected resistance, this study investigates the influence of the differences in pack configurations and module collector positions on the current homogeneity in the pack. Different pack configurations and module collector positions cause the different equivalent connected resistance of each parallel branch, which leads to the current inhomogeneity in the pack [17–19]. The current inhomogeneity seriously reduces the lifetime and safety of the pack [20]. Therefore, quantitatively analyzing the influence of the connected resistance on the current distribution of the pack for different module collector positions is important to optimize the pack performance.

Currently, many studies have investigated the influence of connected resistance on the current distribution of the pack. Research on the parameters that affect the current distribution has been conducted, and the most sensitive parameter was found to be the relationship between the current collected resistance and the cell internal resistance [21,22]. Meanwhile, Hosseinzadeh et al. found that the ratio of connected resistance to internal resistance had the most significant influence on the performance of parallel cell modules compared with the difference in cell capacity and temperature [16]. In addition, they also found that at higher load current and connected resistance, the difference in discharge depth between the cells became more significant, and the temperature gradient increased in the parallel pack, which may cause safety issues [23,24]. Therefore, Chang et al. indicated that the connected resistance was as small as possible and that the module collector was not connected to the edge cell, which could reduce the inhomogeneous current [25]. Li et al. investigated that decreasing connected resistance between the cells mitigated inhomogeneous temperature and reduced inhomogeneous current [26].

Furthermore, the module collector positions also affect the distribution of the connected resistance. Therefore, the current distribution of the pack is inevitably affected by the module collector positions [27]. Zhang et al. found that the state of charge (SOC) and current distribution of the pack were inhomogeneous, and as the distance between the cells and module collectors decreased, the discharge/charge current of the cells increased [28]. Moreover, the cell current closest to the module collectors is the largest, about 3–4 times the average current, which leads to deep discharge and accelerated aging of the cell [18]. Meanwhile, Lv et al. also found that the closer the edge of the module collectors, the greater

the difference between cell currents and the higher the self-balancing loss [22]. Currently, there are two typical pack configurations with different module collector positions: Z and ladder configurations. The Z configuration has a significant advantage over the ladder configuration as it can reduce the influence of interconnect resistance in the parallel module on the differential current [16]. However, the SOC and cell current distribution of the pack are not completely affected by the Z and ladder configurations [29]. Moreover, there is a common module collector position for parallel packs: the middle configuration, in which the positive and negative module collectors are in the middle position of the parallel pack. Rumpf et al. found that it performed better than the ladder configuration [30].

Although the influence of connected resistance on the pack performance has been widely studied, some problems still lack comprehensive and quantitative analysis. Firstly, there is a lack of quantitative analysis of the cell current distribution, and no comprehensive analysis of the causes of the cell current inhomogeneity in the discharge/charge process. Secondly, there is a lack of an approach to reduce the influence of connected resistance on the current homogeneity of the pack using the positions and quantities of module collectors. To quantify the influence of the connected resistance, this study first develops mathematical models of the pack current within different pack configurations and module collector positions to analyze the current distribution at the initial moment. Then, it verifies the mathematical model and quantitatively analyzes the pack current inhomogeneity in the discharge/charge process using COMSOL Multiphysics 6.1 software. Furthermore, this study innovatively proposes the symmetrical multiple module collectors of the pack to greatly improve the current homogeneity of the edge parallel modules.

The main contributions of this paper are as follows:

The mathematical models of the initial cell current distribution within different pack configurations are developed based on the equivalent circuit model, which is not only convenient and time-saving but also accurately quantifies the initial current distribution and provides a guideline for manufacturers to choose the right pack configuration for better performance. Furthermore, the main benefits of the symmetrical multiple module collectors on the current homogeneity of the edge parallel modules are analyzed for the first time, which has important practical significance and provides crucial assistance to manufacturers in improving the lifetime and safety of the pack.

The paper is structured as follows: In Section 2, based on the equivalent circuit model (ECM) of the single cell, a mathematical model of different pack configurations is developed and used to analyze the initial current of cells. In Section 3, COMSOL simulation is implemented to validate the initial cell current distribution and analyze the current difference in the cells in the discharge/charge process. Section 4 quantitatively analyzes the reduction rate of cell current difference in the edge parallel module under multiple module collectors relative to the single module collector using the Dynamic Stress Test (DST) current condition. Finally, the conclusions are presented in Section 5.

2. Pack Configuration and Analytical Model

2.1. 3D Geometric Model

In practice, the cells are mainly connected to a series-parallel pack through the connection topology of the series cell module (SCM) and parallel cell module (PCM). Compared with SCM, PCM has better homogeneity, usable capacity, energy utilization, safety, and economy [31–33]. Therefore, this study develops a 3D geometric model of a series-parallel pack based on the connection topology of PCM. Meanwhile, nickel plates are widely used to connect the cells due to their good weldability, low internal resistance, antioxidant ability, and corrosion resistance [34–36]. Figure 2a shows a common 4p parallel module, which consists of positive and negative nickel plates and four cylindrical batteries, where the positive and negative tabs of the cells are, respectively, connected to the positive and negative nickel plate. The connected nickel plates of the parallel modules are cuboids, as shown in Figure 2b. The different sides of the parallel-module nickel plate can be selected to be connected in series. Therefore, there are two pack configurations with parallel modules in

series: Figure 2c shows the 4p2s pack that the parallel modules are connected to through the long side of the nickel plate (pack configuration 1). Figure 2d shows the 4p2s pack that the parallel modules are connected to through the short side of the nickel plate (pack configuration 2). Based on the above two-pack configurations, this study analyzed the influence of connected resistance on the current homogeneity of series-parallel packs.

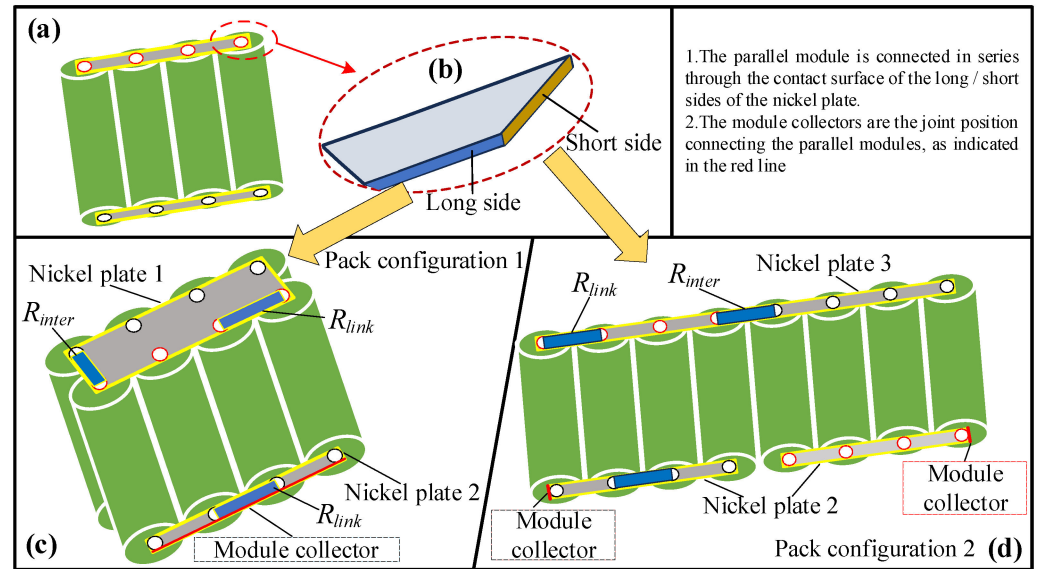


Figure 2. Two pack configurations with the 4p parallel module in series (4p2s pack) by different sides of the nickel plates [29]. (a) 3D geometric model of 4p parallel module. (b) 3D geometric model of nickel plate. (c) 3D geometric model of pack configuration 1. (d) 3D geometric model of pack configuration 2.

2.2. Mathematical Analytical Model

2.2.1. Equivalent Circuit Model

The Thevenin model shown in Figure 3a is selected as the ECM of the cell, which reduces the amount of calculation while satisfying the quantitative analysis of the current. The ECM consists of a voltage source, an RC network, and a constant resistance in series. Based on the above ECM, the expression of the charging and discharging processes of a cell model can be expressed as follows:

$$\begin{cases} U = OCV - IR_0 - U_p \\ U_p = IR_p(1 - e^{-t/\tau}), \\ \tau = R_p C_p \end{cases} \quad (1)$$

where U , OCV , I , R_0 , R_p , C_p , U_p , and τ are the terminal voltage, open-circuit voltage, discharge/charge current, Ohmic resistance, polarization resistance, polarization capacitance, polarization voltage, and time constant of the cell.

2.2.2. ECM of Series-Parallel Pack

The distribution of connected resistance is also different due to the different contract sides of connecting nickel plates. The connected resistance can be obtained by the following equation:

$$R_{link} = \rho \frac{L}{S} \quad (2)$$

where ρ , L , and S are the conductor material resistivity, conductor length, and conductor cross-sectional area. Since the current in the nickel plate mainly flows along the path with the least resistance, the equivalent connected resistance R_{link} and R_{inter} in nickel plate 1 are shown in Figure 2c are almost the same as the corresponding R_{link} and R_{inter} in nickel

plates 2 and 3. In addition, as the distance between the cells in pack configuration 1 and pack configuration 2 is equal, the R_{link} and R_{inter} are roughly the same.

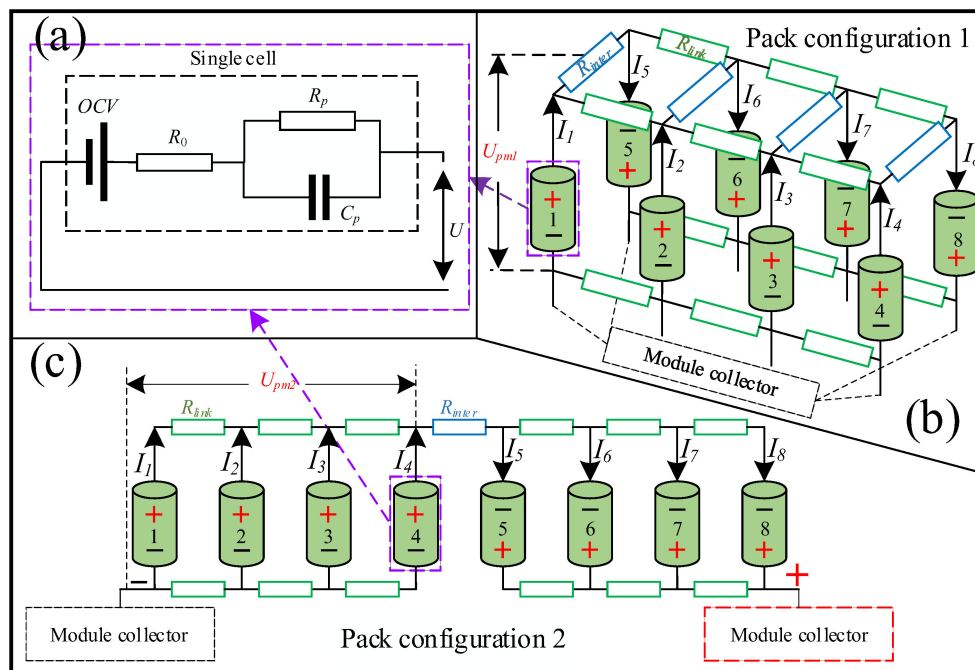


Figure 3. Equivalent circuit models of different pack configurations are developed based on equivalent circuit model of the single cell [29]. (a) Single cell. (b) Pack configuration 1. (c) Pack configuration 2.

Figure 2c,d presents only part of the pack, on which parallel modules can continue to be connected in series in the same way. Therefore, the module collectors are the joint position connecting the parallel modules, as indicated by the red line in Figure 2c,d.

The ECM of pack configuration 1 is shown in Figure 3b. According to Figure 3b, the cell current in the parallel module can be expressed by the following equations:

$$\begin{cases} U_{pm1} = U_1 - \frac{1}{2}I_1R_{inter} = U_2 - \frac{1}{2}I_2R_{inter} = U_3 - \frac{1}{2}I_3R_{inter} = U_4 - \frac{1}{2}I_4R_{inter} \\ U_i = OCV_i - I_iR_i \\ I = \sum_{i=1}^4 I_i \end{cases}, \quad (3)$$

where U_{pm1} and I are the parallel terminal voltage, the pack current, and U_i , I_i , OCV_i and R_i are the terminal voltage, open-circuit voltage, current, and internal resistance of the i th cell. At the beginning of discharging and charging, the battery current is mainly affected by the ohmic resistance. This is because the influence of the polarization resistance on the current appears after the influence of the ohmic resistance on the current. Therefore, the ohmic resistance is considered when calculating the initial current distribution, and the polarization resistance can be regarded as zero. According to Equation (3), the initial cell current distribution in the parallel module can be expressed by the following equations:

$$\frac{OCV - U_{pm1}}{R_0} = I_1 \left(1 + \frac{1}{2} \frac{R_{inter}}{R_0}\right) = I_2 \left(1 + \frac{1}{2} \frac{R_{inter}}{R_0}\right) = I_3 \left(1 + \frac{1}{2} \frac{R_{inter}}{R_0}\right) = I_4 \left(1 + \frac{1}{2} \frac{R_{inter}}{R_0}\right). \quad (4)$$

According to Equation (4), the ratio of the initial discharge current of cells 1 to 4 in the parallel module for pack configuration 1 is

$$I_1 : I_2 : I_3 : I_4 = 1 : 1 : 1 : 1. \quad (5)$$

The ECM of pack configuration 2 is shown in Figure 3c. The cell current in the parallel module can be expressed by the following equations:

$$\begin{cases} U_{pm2} = U_1 - (3I_1 + 2I_2 + I_3)R_{link} \\ U_{pm2} = U_2 - (2I_1 + 3I_2 + 2I_3 + I_4)R_{link} \\ U_{pm2} = U_3 - (I_1 + 2I_2 + 3I_3 + 2I_4)R_{link} \\ U_{pm2} = U_4 - (I_2 + 2I_3 + 3I_4)R_{link} \\ U_i = OCV_i - I_i R_i \\ I = \sum_{i=1}^4 I_i \end{cases} \quad (6)$$

According to Equation (6), the ratio of the initial discharge current of cells 1 to 4 in the parallel module for pack configuration 2 is

$$I_1 : I_2 : I_3 : I_4 = \frac{2\theta + 1}{6\theta^2 + 8\theta + 1} : \frac{1}{6\theta^2 + 8\theta + 1} : \frac{1}{6\theta^2 + 8\theta + 1} : \frac{2\theta + 1}{6\theta^2 + 8\theta + 1}, \quad (7)$$

where U_{pm2} is the parallel terminal voltage, and $\theta = \frac{R_{link}}{R_0}$. According to Equation (7), due to the connected resistance R_{link} , $\theta > 0$. Therefore, the relationship between the initial discharge current of Cell 1 and 4 in the parallel module for pack configuration 2 is

$$I_1 = I_4 > I_2 = I_3, \quad (8)$$

Comparing Equations (5) and (8), it can be concluded that the cell current homogeneity of pack configuration 1 is better than that of pack configuration 2. Homogeneous equivalent connected resistance can be found in each cell parallel branch for pack configuration 1, and the current flowing through each resistance is almost homogeneous. Therefore, a homogeneous voltage drop in the equivalent connected resistance in each parallel branch can be seen, resulting in a homogeneous cell current in each parallel module. In pack configuration 2, although there is homogeneous equivalent connected resistance found for each cell parallel branch, the current flowing through each resistance is inhomogeneous. This makes the voltage drop in the equivalent connected resistances inhomogeneous, resulting in a greater difference in the current between the cells.

Although the current difference between the cells in the parallel module, to a certain extent, can be reflected by the initial current distribution, the difference is not fixed during the discharge process. The polarization resistance and ohmic resistance vary with the constant variations in the cell electrolyte concentration and conductivity in the discharge/charge process, resulting in the varying current distribution of the cells in the parallel module. Varying cell current distributions are difficult to deduce using the mathematical model. Therefore, on the one hand, the COMSOL software is used to verify the mathematical model of the initial current distribution of the cells and analyze the current and voltage distribution in the discharge/charge process, while on the other hand, the COMSOL software is used to research the varying cell current distribution under the DST current condition.

3. Model and Verification

3.1. Construction of 3D Geometric Model

Based on the LG M50T 21,700 lithium-ion battery [29], the 3D geometric models of the packs are shown in Figure 2c,d. The geometric parameters of the pack are shown in Table 1. The nickel plate covers the tabs of the cells at two ends of the parallel module. According to Table 1, the three-dimensional geometric models of the packs are established by COMSOL.

Table 1. Geometric parameters of the 3D model.

Structure	Parameter	Dimension/mm	
Single cell	Length	70	
	Diameter	21	
	Cell distance	2.1	
Nickel plate of parallel module	Nickel plate 1	Length	75.3
		Width	29.1
	Nickel plate 2	Length	75.3
		Width	6
	Nickel plate 3	Length	167.7
		Width	6
Cell tabs	Thickness	0.1	
	Thickness	1	
	Diameter	6	

3.2. Construction of ECM

To study the influence of the connected resistance on the current distribution in the pack, the parameters of each cell in the pack must be kept the same. Therefore, this paper uses experiments to measure a cylindrical lithium-ion battery of LG M50T 21,700 under 25 °C. Subsequently, the multiple cells with the same parameters are generated by simulation to form many 4p parallel modules, which are packed in series into a pack. Among them, the positive and negative electrode materials of the cells are high-density NCA ternary material and Si/C composite material, respectively. The nominal capacity is 4850mAh, and the charge/discharge cut-off voltage is 4.2 V/2.5 V, respectively. The cell nominal capacity is measured by current discharge at $C/3$ until the cut-off voltage. The cell ECM parameters OCV , R_0 , R_p , C_p are all related to SOC. Therefore, the pulse power tests are carried out with 21,700 lithium-ion battery on the test bench to obtain the model parameters. The cell is charged and discharged for 60 s at different current rates (0.2C, 0.5C, 1C) during the pulse power test. The internal resistance of the cell is calculated according to the charge/discharge data, and the cell rests for 30 min at the ambient temperature of 25 °C after each charge/discharge. Then, according to Equation (1), the parameters of the cell ECM are identified by Matlab 2021a using the recursive least squares method. Figure 4a shows the model parameters identified under different SOCs. It is obvious that the R_0 , R_p change little with SOC, so they can be regarded as constant values. The parameters of the cell ECM are shown in Table 2. Moreover, the OCV-SOC curve of the cell ECM is fitted by the data set obtained from the discharging and charging at $C/25$, as shown in Figure 4b.

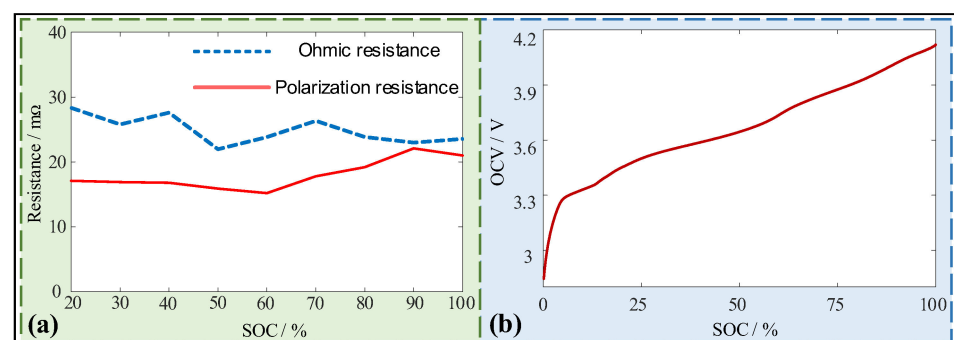


Figure 4. (a) Identified model parameters at different SOCs. (b) OCV-SOC curve measured by experiments [29].

Table 2. Parameters of the cell ECM.

Parameter	Nominal/Ah	Ohmic Resistance/mΩ	Polarization Resistance/mΩ	Time Constant/s
Value	4.82	25.2	17.3	34

3.3. Construction of COMSOL Model

Firstly, the 3D geometric models of the pack are established in COMSOL by the geometric dimensions in Table 1. Secondly, the lumped battery module and the current module are used to simulate the battery characteristics, the current distribution, and flow in the nickel plates, respectively. Meanwhile, they are connected to the corresponding 3D geometric models. Finally, multiple lumped battery modules and current modules are connected by specifying the node positions of the circuit module, and the current source and grounding conditions are set up. The modeling process is shown in Figure 5.

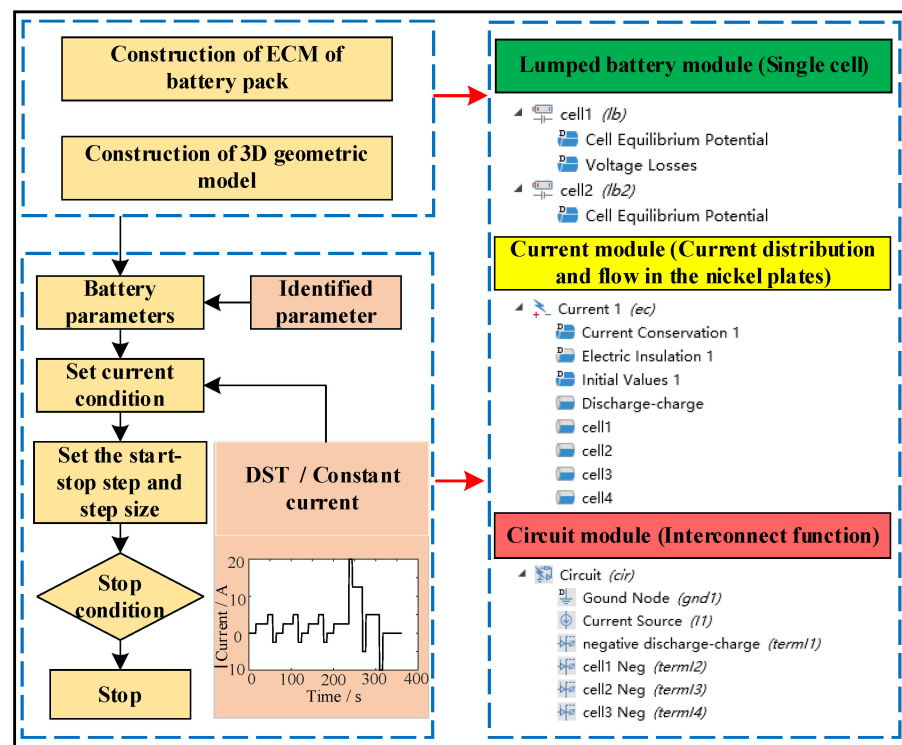


Figure 5. Modeling process of the pack in COMSOL.

3.4. Constant Current Discharge (CCD) Simulation and Analysis of Series-Parallel Pack

In the simulation process, all packs are simulated by CCD, and the initial SOC of each cell is 100%. The discharge stops when the terminal voltage of any cell of the pack reaches the discharge cut-off voltage of 2.5 V. Moreover, the temperature has little effect on the cell resistance and parameters, and other studies do not consider temperature [37,38]. Therefore, the influence of temperature on cell parameters and connected resistance is ignored in the simulation.

To verify the mathematical model of the initial cell current distribution in the parallel module, the calculation values of Equation (7) are compared with the simulation values. As the resistivity of nickel is $6.84 \times 10^{-8} \Omega \cdot m$, and the length, width and thickness are 23.1 mm, 6 mm and 0.1 mm, respectively, the connected resistance R_{link} can be calculated as 2.63 mΩ according to Equation (3), and $\theta = R_{link} / R_0 = 0.10$. Table 3 shows the calculation and simulation value of the initial cell current rate in pack configuration 2. Obviously, the relative error between the calculation and the simulation value is small, which proves the accuracy of Equations (7) and (8).

Table 3. Calculation and simulation value of the initial cell current rate in pack configuration 2.

Single Cell	Cell 1	Cell 2	Cell 3	Cell 4
Calculation value/C	1.09	0.91	0.91	1.09
Simulation value/C	1.07	0.93	0.93	1.07
Relative error	1.87%	2.15%	2.15%	1.87%

The cell current distribution of two pack configurations during the discharge process is shown in Figure 6a. Obviously, the cell current distribution of two pack configurations is different. The cell current of pack configuration 1 is almost homogeneous. However, for pack configuration 2, the currents of cells 1, 4, 5, 8 and cells 2, 3, 6, 7 show different trends, and the difference in current between the cells is constantly varying (the cell number is shown in Figure 3b,c). This is because in the first half of the discharge process, the cell near two ends of the parallel module in pack configuration 2 has the larger discharge and the faster SOC reduction than other cells due to a larger initial discharge current rate. The OCV decreases with the decrease in SOC, resulting in a continuous decrease in the discharge current rate. In the second half of the discharge process, due to the combined influence of OCV and internal resistance, the cell current rate near the two ends of the parallel module firstly increases and then decreases with time, while the cell current rate in the middle of the parallel module firstly decreases and then increases with time.

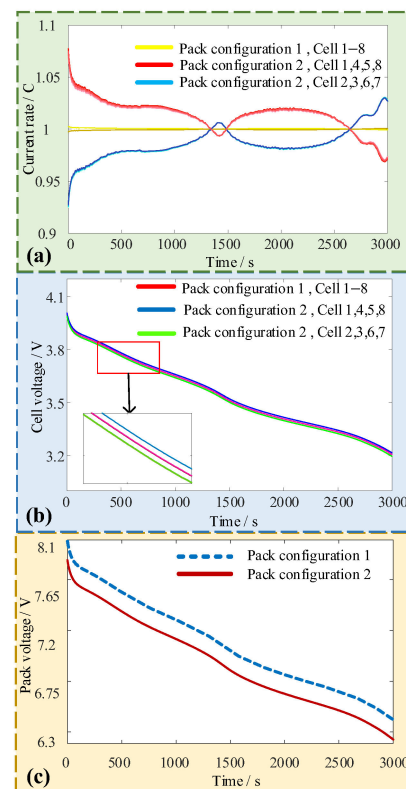


Figure 6. Simulation results of current, voltage and pack voltage distribution of two pack configurations by CCD [29]. (a) Cell current distribution of two pack configurations. (b) Cell voltage distribution of two pack configurations. (c) Pack voltage distribution of two pack configurations.

The cell terminal voltage distribution of two pack configurations is shown in Figure 6b. The cell terminal voltage of pack configuration 1 is nearly a curve, while the cell terminal voltage of pack configuration 2 is two curves with a small gap. This is because the current flowing through the equivalent connected resistance in the parallel module for pack configuration 2 is inhomogeneous, resulting in an inhomogeneous voltage drop in the equivalent connected resistance of each parallel branch. Therefore, there are slight

differences in the cell terminal voltage distribution for pack configuration 2. All in all, the voltage difference between the two pack configurations is very small, which means that the cell current inhomogeneity does not affect the cell terminal voltage distribution.

The pack terminal voltage distribution of two pack configurations is shown in Figure 6c. Compared with pack configuration 1, the pack terminal voltage of pack configuration 1 is significantly lower. This is because the current flow path of pack configuration 2 is longer, which means the voltage loss caused by the connected resistance in the pack for pack configuration 2 is larger, thereby increasing voltage loss, resulting in a low terminal voltage.

Based on the data obtained from the above simulation experiments, the integral operators in COMSOL are used to process the current data results for pack configurations 1 and 2, respectively. The discharge capacity (C_k) of each cell is shown in Table 4. Compared with pack configuration 1, the cell C_k of pack configuration 2 is more inhomogeneous. The inhomogeneous C_k is due to the difference in the current between the cells caused by the connected resistance. Moreover, the pack performance is affected by the C_k inhomogeneity. The worse the C_k inhomogeneity, the greater the influence on the lifetime of the pack.

Therefore, the homogeneity of current, voltage, pack terminal voltage, and C_k for pack configuration 1 is better than those for pack configuration 2. The equivalent connected resistance of each parallel branch is equal by keeping each cell in a parallel module with the same distance to its module collector. In this case, the current homogeneity is improved, which is conducive to improving the overall performance of the pack.

Table 4. Discharge capacity (C_k) of two pack configurations.

Single Cell	1	2	3	4	5	6	7	8
C_k of pack configuration 1/Ah	4.015	4.019	4.019	4.015	4.015	4.019	4.019	4.015
C_k of pack configuration 2/Ah	4.069	3.960	3.962	4.075	4.070	3.964	3.963	4.072

4. Result and Discussion

4.1. Analysis of Series-Parallel Pack

To further analyze the cell current and voltage distribution under complex current conditions, based on the above analysis results, the 4p8s series-parallel battery was constructed by pack configuration 1, as shown in Figure 7a. Based on the DST condition shown in Figure 7b, the current and voltage of the pack are simulated and analyzed by COMSOL software, where the negative/positive module collector positions are located on the short side of the negative nickel plate of Cell 1 and the short side of the positive nickel plate of Cell 32, respectively. The intermediate module collectors are the positions where the non-edge parallel module is connected, as shown by the blue line in Figure 7a.

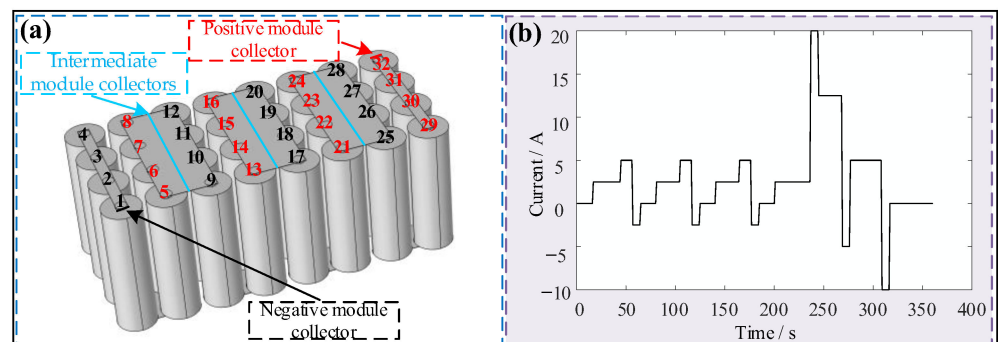


Figure 7. (a) 3D geometric model of 4p8s pack. (b) Dynamic Stress Test current condition diagram.

The cell current and voltage distribution are obtained by simulation, as shown in Figure 8a,b. Compared with the non-edge parallel modules, the cell current homogeneity

of the edge parallel module in the pack is significantly worse. For the edge parallel module, the cell farther from the positive/negative module collectors has the larger equivalent connected resistance, which leads to a smaller cell current rate. For the non-edge parallel module, the distance between the cells in the parallel module and the intermediate module collectors is equal, which makes the equivalent connected resistances of each parallel branch equal. Therefore, the cell current homogeneity is better.

As shown in Figure 8a and Table 5, according to the DST current condition, the higher the charge/discharge current rate, the greater the current difference between the cells (i.e., the worse the current homogeneity). During the period of the maximum charge-discharge current rate (i.e., 237–244 s), the charge/discharge current rate of cell 1 and 32 closest to the module collectors is largest, followed by cell 2 and 31, cell 3 and 30, cell 4 and 29. Among them, the current difference between cell 29 and 32 is the largest, and the current of cell 32 is 43.97% higher than cell 29, while the current homogeneity of the cells (cell 5–28) in the non-edge parallel module is better. Moreover, the current of cell 32 in the edge parallel module is 21.80% higher than the average current of the cell 5–28. Figure 9 shows the cell current distribution of the pack at 238 s, which can clearly reflect the current difference between the cells.

Table 5. The cell current during the period of the maximum charge–discharge current rate.

Moment/s	Cell 5–28 (Average Current)/A	Cell 29 Current/A	Cell 32 Current/A
237	4.83	4.07	5.90
238	5.00	4.23	6.09
239	5.00	4.24	6.08
240	5.00	4.25	6.06
241	5.00	4.26	6.04
242	5.00	4.27	6.02
243	4.93	4.23	5.93
244	4.67	4.02	5.58

The cell voltage distribution in the parallel module of the pack is shown in Figure 8b. Comparing Figure 8a,b, the cell voltage and current distribution in the parallel module are similar. The cell voltage homogeneity of the edge parallel modules is worse than that of the non-edge parallel modules. The parallel voltage of the edge parallel modules is homogeneous. The cell farther from the positive/negative module collector has a larger voltage drop on the equivalent connected resistances, which leads to a smaller cell voltage. For the non-edge parallel modules, the equivalent connected resistances in each parallel branch are equal. Therefore, cell voltage homogeneity is better.

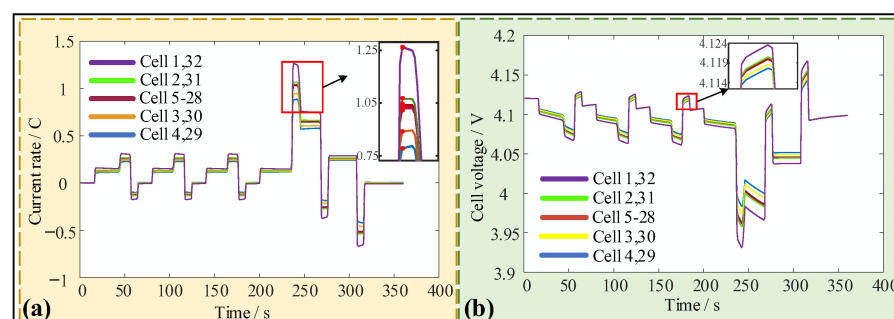


Figure 8. Simulation results of current and voltage distribution of 4p8s pack by Dynamic Stress Test current condition discharge/charge. (a) Current distribution of 4p8s pack. (b) Voltage distribution of 4p8s pack.

Based on the above analysis, the module collector positions have a greater influence on the current and voltage distribution of the edge parallel modules than on the non-edge

parallel modules in the pack. The main reason is that the module collector positions lead to unequal equivalent connected resistances of each branch in the edge parallel modules, which in turn affects the cell current and voltage. For the non-edge parallel module, the current and voltage homogeneity is better due to the equal equivalent connected resistances of each parallel branch.

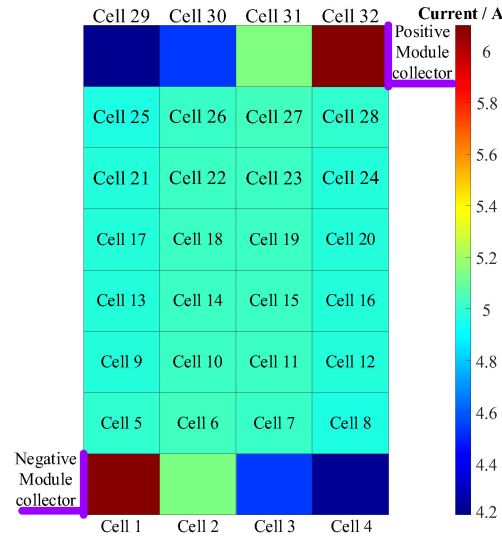


Figure 9. Cell current distribution of the pack for DST condition at 238 s (as indicated in the red dots in Figure 8).

4.2. Pack of Multiple Module Collectors

To further improve cell current homogeneity of the edge parallel module in the pack, the influence of the symmetrical multiple module collectors on the current homogeneity is explored. The negative module collectors are located on the short side of the negative nickel plates of cells 1 and 4, and the positive module collectors are located on the short side of the positive nickel plates of cells 29 and 32, as shown in Figure 10a. According to the mathematical model of the initial current distribution, the ratio of the initial discharge currents of cells 1 to 4 in the edge parallel module is.

$$I_1 : I_2 : I_3 : I_4 = \frac{\theta^3 + 5\theta^2 + 6\theta + 2}{\theta^3 + 5\theta^2 + 6\theta + 1} : \frac{\theta^2 + 4\theta + 2}{\theta^3 + 5\theta^2 + 6\theta + 1} : \frac{\theta^2 + 4\theta + 2}{\theta^3 + 5\theta^2 + 6\theta + 1} : \frac{\theta^3 + 5\theta^2 + 6\theta + 2}{\theta^3 + 5\theta^2 + 6\theta + 1} \quad (9)$$

So, the relationship between the initial discharge current of cells 1 and 4 in the parallel module is.

$$I_1 = I_4 > I_2 = I_3. \quad (10)$$

Meanwhile, the initial cell current distribution of the edge parallel module under the single/double module collectors is shown in Table 6, where the single module collector refers to only a pair of positive/negative module collectors, and double module collectors refer to two pairs of positive/negative module collectors. Compared with the single module collector, cell current homogeneity in the edge parallel modules of double module collectors is significantly better. This is because symmetrical module collectors of the pack make the distribution of the equivalent connected resistance in the edge parallel module more homogeneous, thereby reducing the current inhomogeneity of the edge parallel module.

The cell current distribution of the double module collectors is shown in Figure 11a. Comparing Figures 8a and 11a, the current of cells 1 to 4 and cells 29 to 32 is almost homogeneous during the period of the small discharge/charge current rate. However, compared with the single module collector, the current difference between the cells in the edge parallel module of the double module collectors is significantly smaller during the period of large discharge/charge current rates. The maximum cell current difference $K_c = (I_{max} - I_{min})/I_{min}$ in the edge parallel module of the single/double module collectors

during the maximum charge/discharge current rate period (i.e., 237–244 s) is shown in Table 7. It can be found that the cell current inhomogeneity in the edge parallel module of the double module collectors is significantly improved during this period, and the current homogeneity is increased by 84.90% relative to the single module collector.

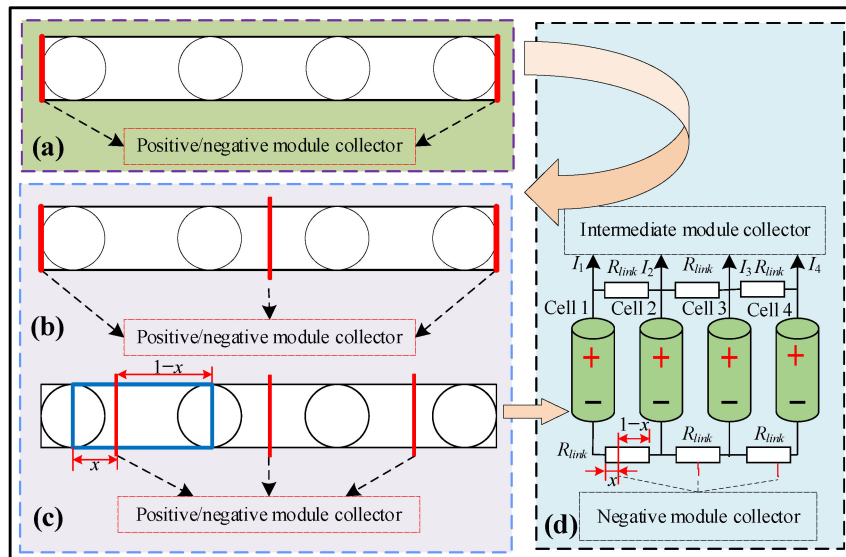


Figure 10. Distribution of n pairs of module collectors ($n = 2, 3$) of positive and negative nickel plates. (a) Distribution of double module collector. (b) 2D geometric model of arrangement mode 1. (c) 2D geometric model of arrangement mode 2. (d) Equivalent circuit model of edge parallel module.

Table 6. Initial cell current distribution of the edge parallel module under single/double module collectors.

Quantity of Module Collector		Cell 1	Cell 2	Cell 3	Cell 4
Current/A	Single module collector	0.025	0.019	0.016	0.015
	Double module collectors	0.028	0.026	0.026	0.028

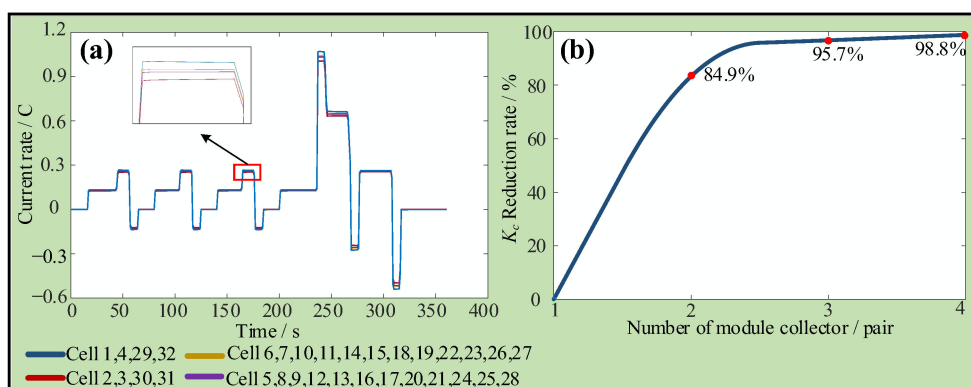


Figure 11. (a) Cell current distribution of double module collectors. (b) K_c reduction rate in the edge parallel module of n pairs of module collectors relative to the single module collector ($n = 2, 3, 4$).

In addition, the influence of the symmetrical distribution of the n pairs of module collectors on the current homogeneity is further explored. The module collectors located on two short-sides of the nickel plates remain unchanged, and the remaining module collectors are evenly distributed in the middle of the nickel plate. The distribution of the three pairs of module collectors is shown in Figure 8b. The distribution mode of the module collectors is called arrangement mode 1. Since the module collector is a rectangle with a very small

width, it can be regarded as a line. The distribution of other n pairs of module collectors is similar to that of three pairs of module collectors.

Table 7. Maximum cell current difference K_c in the edge parallel module of single/double module collectors.

Quantity of Module Collector	Single Cell	Current/A	K_c
Single module collector	Cell 29	4.23	43.97%
	Cell 32	6.09	
Double module collectors	Cell 29	5.14	6.64%
	Cell 30	4.82	

The K_c reduction rate in the edge parallel module of n pairs of module collectors relative to the single module collector is shown in Figure 11b. According to Figure 11b, the K_c reduction rate of the edge parallel module continues to increase with the increase in the quantities of module collectors, but the rising magnitude of the K_c reduction rate continues to decrease. For example, compared with the single module collector, the K_c in the edge parallel module of the two pairs of module collectors is reduced by 84.90%. However, the K_c reduction rate of the three pairs of module collectors relative to the two pairs of module collectors is only 10.80% higher.

In addition to the above arrangement mode 1, another distribution of the three pairs of module collectors (i.e., arrangement mode 2) is shown in Figure 10c. All the module collectors are distributed in the middle of the nickel plate. The purpose of this distribution is to make the equivalent connected resistance of each cell's parallel branch equal. The ECM of the edge parallel module for arrangement mode 2 is shown in Figure 10d. The equivalent connected resistances of each parallel branch can be expressed by the following equations.

$$\begin{cases} R_1 = R_4 = xR_{link}, 0 \leq x \leq 1 \\ R_2 = R_3 = \frac{1}{\frac{1}{(1-x)R_{link}} + \frac{1}{R_{link}/2}} \end{cases} \quad (11)$$

where R_i is the equivalent connected resistance of the branch where i th cell is located, and x is the equivalent connected resistance division ratio caused by the module collectors, as shown in Figure 10d. According to Equation (11), as $x = 0.29$, the equivalent connected resistance of each parallel branch is equal, which can significantly reduce the current difference between the cells in the edge parallel module. After simulation verification, the K_c in the edge parallel module of the three pairs of module collectors relative to the single module collector is reduced by 99.66% for arrangement mode 2.

Therefore, the cell current homogeneity of the edge parallel module is not only related to the quantities of module collectors but also to the positions of the module collector. However, it is impossible to find the best position to make the equivalent connected resistance of each branch equal for some quantities of the module collectors. For example, Figure 12 shows the distribution of three pairs of module collectors based on the 5p parallel module. This distribution can only make the equivalent connected resistance of the parallel branches where cells 1, 2, 4, and 5 are located equal. Therefore, it is recommended to select the appropriate quantities of module collectors according to the quantities of parallel cells. Furthermore, although the more module collectors, the smaller the K_c of the edge parallel module, the increase in magnitude of the K_c reduction rate continues to decrease, increasing pack complexity and the cost of the pack. Therefore, the optimal positions of module collectors should be sought under smaller quantities of module collectors.

4.3. Limitations and Future Work

Quantitative analysis of the influence of the connected resistance on the current distribution and the improvement in the current inhomogeneity of the pack are the main topics of this study. The coupling of multiple influencing factors increases the complexity

of the research. Therefore, this study does not consider these influencing factors, such as temperature, cell-to-cell variations, dynamic internal resistance, etc.

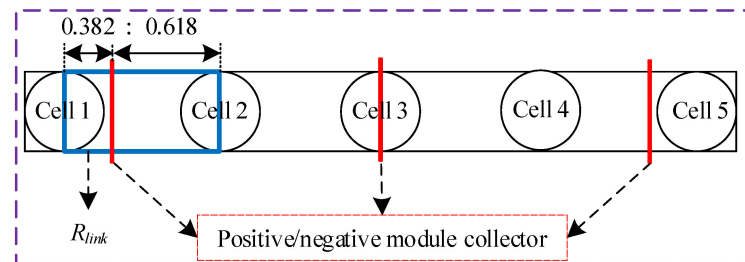


Figure 12. Distribution of three pairs module collectors.

Based on the model and methodology of this study, we consider adding temperature conditions and heating under the low-temperature conditions to the pack in future work. Meanwhile, we aim to further explore the influence of temperature on current distribution and seek better methods to reduce temperature effects.

5. Conclusions

To analyze the influence of connected resistance on the current distribution within the different pack configurations and module collector positions, this study chooses two different pack configurations with parallel modules in series: the long-side pack and the short-side pack. According to the equivalent circuit model (ECM), the initial cell current distribution in the parallel module was theoretically deduced and quantitatively analyzed. Then, COMSOL software was used to verify the mathematical model of initial cell current distribution and analyze the voltage and current distribution in the constant current discharge (CCD) process. Moreover, the current distribution of the pack constructed by the long-side pack with better performance under complex current conditions was further studied. Meanwhile, the influence of multiple module collectors on the current homogeneity of the edge parallel module was explored.

The results show that the cell current homogeneity in the parallel module of the long-side pack is better than that of the short-side pack at the initial discharge moment. In the CCD process, the cell current of the long-side pack is homogeneous, while there is a significant current difference between the cells near the module collector and the cells further away from the module collector for the short-side pack. According to the simulation results of complex current conditions, the module collector positions mainly affect the current homogeneity of the edge parallel module in the pack, while the non-edge parallel module is almost unaffected. Moreover, the multiple module collectors can effectively reduce the maximum current difference between the cells of the edge parallel module, and its reduction rate is not only related to the quantities of module collectors but also to the module collector positions. Therefore, considering the pack complexity, the cost of the pack, and the rising magnitude of the reduction rate of the maximum cell current difference in the edge parallel module caused by multiple module collectors, it is recommended to seek the optimal positions of module collectors under smaller quantities of module collectors for manufacturers.

Author Contributions: Conceptualization, Z.Y., Z.S. and L.C.; methodology, Z.Y. and Z.S.; software, Z.S. and C.L. (Chunxiao Luan); validation, Z.Y. and Z.S.; formal analysis, Z.Y. and Z.S.; investigation, Z.S.; resources, Z.Y. and H.L.; data curation, Z.S.; writing—original draft preparation, Z.Y. and Z.S.; writing—review and editing, L.C., C.M., C.L. (Changlong Li) and M.Y.M.A.-s.; visualization, Z.S.; supervision, L.C.; project administration, L.C.; funding acquisition, L.C. and H.L. All authors have read and agreed to the published version of the manuscript.

Funding: This research was funded by the Open Foundation of the Key Laboratory of Marine Environmental Survey Technology and Application, Ministry of Natural Resources (MESTA-2020-B002), the National Natural Science Foundation of China (No. 62103242, 62273213, 61633015, 62133007,

U1964207, U1864205, U1764258), Youth Innovation Team of universities in Shandong Province (No. 2022KJ221), and Natural Science Foundation of Shandong Province for Innovation and Development Joint Funds (No. ZR2022LZH001).

Data Availability Statement: Not applicable.

Conflicts of Interest: The authors declare no conflict of interest.

References

1. Hannan, M.A.; Hoque, M.M.; Hussain, A.; Yusof, Y.; Ker, P.J. State-of-the-Art and Energy Management System of Lithium-Ion Batteries in Electric Vehicle Applications: Issues and Recommendations. *IEEE Access* **2018**, *6*, 19362–19378. [\[CrossRef\]](#)
2. Li, J.; Li, L.; Li, Z.; Jiang, Z.; Gu, J. Co-estimation of parameters and state of charge for lithium-ion battery. *J. Electroanal. Chem.* **2022**, *907*, 116011. [\[CrossRef\]](#)
3. Rogers, D.J.; Aslett, L.J.M.; Troffaes, M.C.M. Modelling of modular battery systems under cell capacity variation and degradation. *Appl. Energy* **2021**, *283*, 116360. [\[CrossRef\]](#)
4. Wang, J.; Zhang, S.; Hu, X. A Fault Diagnosis Method for Lithium-Ion Battery Packs Using Improved RBF Neural Network. *Front. Energy Res.* **2021**, *9*, 702139. [\[CrossRef\]](#)
5. Madani, S.S.; Soghrati, R.; Ziebert, C. A Regression-Based Technique for Capacity Estimation of Lithium-Ion Batteries. *Batteries* **2022**, *8*, 31. [\[CrossRef\]](#)
6. Venet, P. Battery Performance, Ageing, Reliability and Safety. *Batteries* **2023**, *9*, 277. [\[CrossRef\]](#)
7. Duffner, F.; Kronemeyer, N.; Tübke, J.; Leker, J.; Winter, M.; Schmich, R. Post-lithium-ion battery cell production and its compatibility with lithium-ion cell production infrastructure. *Nat. Energy* **2021**, *6*, 123–134. [\[CrossRef\]](#)
8. Ebner, M.; Marone, F.; Stapanoni, M.; Wood, V. Visualization and Quantification of Electrochemical and Mechanical Degradation in Li Ion Batteries. *Science* **2013**, *342*, 716–720. [\[CrossRef\]](#)
9. Mahmoudzadeh Andwari, A.; Pesiridis, A.; Rajoo, S.; Martinez-Botas, R.; Esfahanian, V. A review of Battery Electric Vehicle technology and readiness levels. *Renew. Sustain. Energy Rev.* **2017**, *78*, 414–430. [\[CrossRef\]](#)
10. Dubarry, M.; Vuillaume, N.; Liaw, B.Y. Origins and accommodation of cell variations in Li-ion battery pack modeling. *Int. J. Energy Res.* **2010**, *34*, 216–231. [\[CrossRef\]](#)
11. Santhanagopalan, S.; White, R.E. Quantifying Cell-to-Cell Variations in Lithium Ion Batteries. *Int. J. Electrochem.* **2012**, *2012*, 395838. [\[CrossRef\]](#)
12. Chang, L.; Ma, C.; Zhang, C.; Duan, B.; Cui, N.; Li, C. Correlations of lithium-ion battery parameter variations and connected configurations on pack statistics. *Appl. Energy* **2023**, *329*, 120275. [\[CrossRef\]](#)
13. Pordanjani, A.H.; Aghakhani, S.; Afrand, M.; Zhang, P.; Tang, R.; Mahian, O.; Wongwises, S.; Rashidi, M.M. Thermo-electrochemical simulation of the cooling process in a compact battery pack considering various configurations. *J. Power Sources* **2023**, *553*, 232112. [\[CrossRef\]](#)
14. Liu, X.; Ai, W.; Naylor Marlow, M.; Patel, Y.; Wu, B. The effect of cell-to-cell variations and thermal gradients on the performance and degradation of lithium-ion battery packs. *Appl. Energy* **2019**, *248*, 489–499. [\[CrossRef\]](#)
15. Song, Z.; Yang, N.; Lin, X.; Pinto Delgado, F.; Hofmann, H.; Sun, J. Progression of cell-to-cell variation within battery modules under different cooling structures. *Appl. Energy* **2022**, *312*, 118836. [\[CrossRef\]](#)
16. Hosseinzadeh, E.; Arias, S.; Krishna, M.; Worwood, D.; Barai, A.; Widanalage, D.; Marco, J. Quantifying cell-to-cell variations of a parallel battery module for different pack configurations. *Appl. Energy* **2021**, *282*, 115859. [\[CrossRef\]](#)
17. Shang, Y.; Zhu, C.; Fu, Y.; Mi, C.C. An Integrated Heater Equalizer for Lithium-Ion Batteries of Electric Vehicles. *IEEE Trans. Ind. Electron.* **2019**, *66*, 4398–4405. [\[CrossRef\]](#)
18. Wang, L.; Cheng, Y.; Zhao, X. Influence of connecting plate resistance upon LiFePO₄ battery performance. *Appl. Energy* **2015**, *147*, 353–360. [\[CrossRef\]](#)
19. Wu, B.; Yufit, V.; Marinescu, M.; Offer, G.J.; Martinez-Botas, R.F.; Brandon, N.P. Coupled thermal–electrochemical modelling of uneven heat generation in lithium-ion battery packs. *J. Power Sources* **2013**, *243*, 544–554. [\[CrossRef\]](#)
20. Offer, G.J.; Yufit, V.; Howey, D.A.; Wu, B.; Brandon, N.P. Module design and fault diagnosis in electric vehicle batteries. *J. Power Sources* **2012**, *206*, 383–392. [\[CrossRef\]](#)
21. Grün, T.; Stella, K.; Wollersheim, O. Influence of circuit design on load distribution and performance of parallel-connected Lithium ion cells for photovoltaic home storage systems. *J. Energy Storage* **2018**, *17*, 367–382. [\[CrossRef\]](#)
22. Lv, J.; Lin, S.; Song, W.; Chen, M.; Feng, Z.; Li, Y.; Ding, Y. Performance of LiFePO₄ batteries in parallel based on connection topology. *Appl. Energy* **2019**, *252*, 113407. [\[CrossRef\]](#)
23. Hosseinzadeh, E.; Marco, J.; Jennings, P. Combined electrical and electrochemical-thermal model of parallel connected large format pouch cells. *J. Energy Storage* **2019**, *22*, 194–207. [\[CrossRef\]](#)
24. Hosseinzadeh, E.; Odio, M.X.; Marco, J.; Jennings, P.A. Unbalanced Performance of Parallel Connected Large Format Lithium Ion Batteries for Electric Vehicle Application. In Proceedings of the 2019 International Conference on Smart Energy Systems and Technologies (SEST), Porto, Portugal, 9–11 September 2019; pp. 1–6.

25. Chang, L.; Duan, B.; Li, P.; Zhang, K.; Zhang, C.; Xiao, L. In Influence of interconnect resistances on parallel-connected LiFePO₄ cells performance. In Proceedings of the 2019 3rd Conference on Vehicle Control and Intelligence (CVCI), Hefei, China, 21–22 September 2019; pp. 1–4.
26. Li, Y.; Lan, B.; Luo, J. In Modeling and Simulation Evaluation of Current and Temperature Inconsistency in Parallel Connected Lithium-Ion Batteries. In Proceedings of the 2018 International Conference on Information Systems and Computer Aided Education (ICISCAE), Changchun, China, 6–8 July 2018; pp. 12–18.
27. Baumann, M.; Wildfeuer, L.; Rohr, S.; Lienkamp, M. Parameter variations within Li-Ion battery packs—Theoretical investigations and experimental quantification. *J. Energy Storage* **2018**, *18*, 295–307. [[CrossRef](#)]
28. Zhang, Y.; Zheng, J.; Lin, S.; Bai, F.; Tanveer, W.H.; Cha, S.; Wu, X.; Feng, W. Nonuniform current distribution within parallel-connected batteries. *Int. J. Energy Res.* **2018**, *42*, 2835–2844. [[CrossRef](#)]
29. Chang, L.; Ma, C.; Luan, C.; Sun, Z.; Wang, C.; Li, H.; Zhang, Y.; Liu, X. Influence of the Assembly Method on the Cell Current Distribution of Series–Parallel Battery Packs Based on Connector Resistance. *Front. Energy Res.* **2022**, *10*, 804303. [[CrossRef](#)]
30. Rumpf, K.; Rheinfeld, A.; Schindler, M.; Keil, J.; Schua, T.; Jossen, A. Influence of cell-to-cell variations on the inhomogeneity of lithium-ion battery modules. *J. Electrochem. Soc.* **2018**, *165*, A2587. [[CrossRef](#)]
31. Brand, M.J.; Hofmann, M.H.; Steinhardt, M.; Schuster, S.F.; Jossen, A. Current distribution within parallel-connected battery cells. *J. Power Sources* **2016**, *334*, 202–212. [[CrossRef](#)]
32. Luan, C.; Ma, C.; Wang, C.; Chang, L.; Xiao, L.; Yu, Z.; Li, H. Influence of the connection topology on the performance of lithium-ion battery pack under cell-to-cell parameters variations. *J. Energy Storage* **2021**, *41*, 102896. [[CrossRef](#)]
33. Plett, G.L.; Klein, M.J. In Simulating Battery Packs Comprising Parallel Cell Modules and Series Cell Modules. In Proceedings of the EVS 24, Stavanger, Norway, 13–16 May 2009.
34. Brand, M.J.; Schmidt, P.A.; Zaeh, M.F.; Jossen, A. Welding techniques for battery cells and resulting electrical contact resistances. *J. Energy Storage* **2015**, *1*, 7–14. [[CrossRef](#)]
35. Sadeghian, A.; Iqbal, N. A review on dissimilar laser welding of steel-copper, steel-aluminum, aluminum-copper, and steel-nickel for electric vehicle battery manufacturing. *Opt. Laser Technol.* **2022**, *146*, 107595. [[CrossRef](#)]
36. Shui, L.; Chen, F.; Garg, A.; Peng, X.; Bao, N.; Zhang, J. Design optimization of battery pack enclosure for electric vehicle. *Struct. Multidiscip. Optim.* **2018**, *58*, 331–347. [[CrossRef](#)]
37. Fill, A.; Koch, S.; Pott, A.; Birke, K.-P. Current distribution of parallel-connected cells in dependence of cell resistance, capacity and number of parallel cells. *J. Power Sources* **2018**, *407*, 147–152. [[CrossRef](#)]
38. Fill, A.; Koch, S.; Birke, K.P. Analytical model of the current distribution of parallel-connected battery cells and strings. *J. Energy Storage* **2019**, *23*, 37–43. [[CrossRef](#)]

Disclaimer/Publisher’s Note: The statements, opinions and data contained in all publications are solely those of the individual author(s) and contributor(s) and not of MDPI and/or the editor(s). MDPI and/or the editor(s) disclaim responsibility for any injury to people or property resulting from any ideas, methods, instructions or products referred to in the content.